Acta Cryst. (1999). B**55**, 902–916

Charge distribution as a tool to investigate structural details: meaning and application to pyroxenes

Massimo Nespolo,[a]* Giovanni Ferraris[b] and Haruo Ohashi[a]

[a]*National Institute for Research in Inorganic Materials, Research Center for Creating New Materials, 1-1 Namiki, Tsukuba-shi, Ibaraki 305-0044, Japan, and* [b]*Department of Mineralogical and Petrologic Sciences, University of Torino, Via Valperga Caluso 35, 10125 Torino, Italy. E-mail: nespolo@nirim.go.jp*

(*Received 5 May 1999; accepted 28 June 1999*)

Abstract

The charge distribution (CD) method, previously introduced as a development of the bond-valence (BV) approach, is applied for the first time to mineral structures, and specifically to pyroxenes. CD essentially involves the distribution of the Effective Coordination Number (ECoN) of a cation among all the neighboring anions. This distribution is then interpreted in terms of distribution of 'charges', where 'charge' represents the formal oxidation state. Differently from BV, the CD description depends upon the geometry of each coordination polyhedron, which is characterized through ECoN (a non-integer number). The contribution of each cation–oxygen bond to ECoN, labelled 'bond weight', corresponds to the bond strength in the BV method, but it is defined in terms of bond-length ratio in each polyhedron and not as a function of the cation–oxygen pair. The ratio q/Q of the formal oxidation number to the computed charge can be interpreted as a measure of the correctness of the structure (cation ratio) and of the degree of over- or under-bonding (anion ratio). A similar interpretation is not possible for the analogous quantities obtained through the BV approach. The analysis in terms of CD of the pyroxene chains (from 101 structures) shows different trends as a function of composition, temperature and pressure; in particular it shows a different behaviour of the two crystallographically independent chains of orthopyroxenes and of $P2_1/c$ clinopyroxenes.

1. Introduction

Pauling's definition of *bond strength* (Pauling, 1929) is based upon the idea of interpreting the bond length as the sum of ionic radii. It is defined as the ratio valence/(coordination number) of a given cation and is strictly applicable only to structures with regular or quasi-regular coordination polyhedra.

When non-ionic bonds are involved, the availability of orbitals, rather than the ratio of cation and anion radii, governs the coordination (Brown, 1988; Chiari, 1988). In this context, the terms 'cation' and 'anion' are not rigorously correct and hereinafter they are used with reference to the formal oxidation state of an atom. Baur (1970, 1971) showed a linear dependence of the bond length from the total Pauling's bond strength (p) received by *each* anion (*cf.* also Ferraris & Catti, 1973). In case of very distorted distributions (*e.g.* those around V^{5+}), however, the results are poor (Gopal, 1972).

The bond strength s, computed from the experimental set of bond lengths through the so-called '*R-s* curves' (Donnay & Allman, 1970; Pyatenko, 1973; Brown & Shannon, 1973; Brown & Wu, 1976; Allman, 1975; Trömel, 1983, 1984, 1986; Brown & Altermatt, 1985; *cf.* also Gibbs *et al.*, 1998, for other references), is termed *bond valence* (Donnay & Allman, 1970). The *R-s* curves are not linear and contain empirical parameters that have been fitted on a large set of refined structures. The coordination number is the number of anions after which s is close to zero (Brown, 1978), but it has been set *a priori* in the group of structures used for determining the empirical parameter. Brown (1977, 1978) developed the theory of bond valence as a method of predicting bond lengths in inorganic crystals and the *R-s* curves based on his approach are widely used.

Hoppe (1979) criticized the common definition and applications of the concepts on which BV theory is based, namely:

(i) *the coordination number*, which can be hardly identified in those cases in which no net separation appears between a first and a second coordination sphere (Chiari, 1990; Balić Žunić & Makovicky, 1996; Makovicky & Balić Žunić, 1998);

(ii) *the ionic radius*, because the interatomic distances are not always describable as the sum of ionic radii.

To generalize the concepts of coordination number and ionic radius, Hoppe (1979) introduced the definitions of FIR (Fictive Ionic Radii), MEFIR (MEan Fictive Ionic Radii) and ECoN (Effective Coordination Number), and Hoppe *et al.* (1989) applied ECoN to the calculation of the distribution of charges in crystalline structures. This 'charge' actually has a strict correspondence with the BV, as defined by Brown (1978). Hoppe

et al. (1989) showed that the charge distribution (hereinafter CD) method systematically gives better results than BV when applied to oxide compounds.

In this paper we compare the CD and the BV methods analyzing their meanings and implications. An application of the CD method to pyroxenes shows that, with well refined structures, CD is a parameter suitable for detecting subtle structural variations as a function of the composition, temperature and pressure. A Fortran computer program (*CHARDIS*99) to calculate CD and three types of BV curves (Brown & Shannon, 1973; Brown & Wu, 1976; Brown & Altermatt, 1985) is available on request from the first author.

2. Comparison of CD and BV methods

Applying Hoppe *et al.* (1989) symbolism, hereinafter $q(ij)$ and $Q(ij)$ indicate the formal oxidation state and computed BV or charge for the cation of the ith chemical species and of jth crystallographic type (termed the ijth cation henceforth). Similarly, $q(k)$ and $Q(k)$ indicate the formal oxidation state and computed BV or charge for the oxygen of the k crystallographic type (termed the kth oxygen henceforth). Then, $d(ij \rightarrow k)_l$ is the lth distance (increasing with l) between the kth oxygen and the ijth cation, and $n(ij \rightarrow k)_l$ is the corresponding multiplicity.

For the BV method, Brown & Shannon (1973) introduced the curve

$$s(ij \rightarrow k)_l = s_0[d(ij \rightarrow k)_l/R_0]^{-N} \tag{1}$$

to calculate the bond valence $s(ij \rightarrow k)_l$ for the bond with length $d(ij \rightarrow k)_l$. In (1) there are three types of empirical parameters: R_0, close to the mean cation–oxygen distance, which we term the *normalizing parameter*; N, which we term the *contraction parameter*; s_0, close to p (the total Pauling's bond strength), which we term the *scaling parameter*. All these parameters are characteristic of the cation–anion pair. The total BV is computed as

$$Q(k) = -\sum_i \sum_j \sum_l s(ij \rightarrow k)_l n(ij \rightarrow k)_l [h(ij)/h(k)] \tag{2a}$$

$$Q(ij) = \sum_k \sum_l s(ij \rightarrow k)_l n(ij \rightarrow k)_l, \tag{2b}$$

where h is the multiplicity of the Wyckoff position. The multiplicity ratio $h(ij)/h(k)$ in the computation of $Q(k)$ removes multiple contributions from $d(ij \rightarrow k)_l$ which are equivalent by symmetry. It does not enter in the computation of $Q(ij)$, because also equivalent $d(ij \rightarrow k)_l$ contribute to the coordination sphere of the ijth cation.

In the CD method the (weighted) mean cation–oxygen distance $[d(ij \rightarrow O)]$ and ECoN $[E'(ij)]$ are defined as

$$d(ij \rightarrow O) = \left(\sum_k \sum_l d(ij \rightarrow k)_l n(ij \rightarrow k)_l \exp\{1 - [d(ij \rightarrow k)_l/d(ij \rightarrow k)_1]^6\} \right) / \left(\sum_k \sum_l n(ij \rightarrow k)_l \exp\{1 - [d(ij \rightarrow k)_l/d(ij \rightarrow k)_1]^6\} \right) \tag{3}$$

$$E'(ij) = \sum_k \sum_l \exp\{1 - [d(ij \rightarrow k)_l/d(ij \rightarrow O)]^6\}. \tag{4}$$

The exponent 6 was empirically determined on a set of test structures and corresponds to a contraction parameter, as defined above. This exponent is the only empirical parameter used: it is characteristic of the oxygen anion and does not depend upon the cation. $E'(ij)$ (ECoN) is a *non-integer* number (except for regular polyhedra), giving a sort of 'weighted' coordination number, which in some respects is reminiscent of the 'average coordination number' of non-crystalline solids (Phillips, 1980; Thorpe, 1983). Restriction to an integer coordination number severely hinders the application of the bond-strength/bond-valence approach to structures in which the coordination is irregular. A typical example is the case of the $M1$ and $M2$ sites of pyroxenes, for which Ferguson (1974) showed that a satisfactory distribution of BV is obtained only assuming non-realistic coordination numbers.

The contribution of each bond to ECoN is labelled here as *bond weight* and is expressed as

$$w(ij \rightarrow k)_l = \exp\{1 - [d(ij \rightarrow k)_l/d(ij \rightarrow O)]^6\}. \tag{5}$$

The contribution of each O atom to ECoN of the ijth cation is the sum of the bond weights

$$\Delta E'(ij \rightarrow k) = \left[\sum_l w(ij \rightarrow k)_l \right] / E'(ij). \tag{6}$$

$Q(k)$ and $Q(ij)$ are then calculated as (original equations have been rearranged)

$$Q(k) = -\sum_i \sum_j \Delta E'(ij \rightarrow k) q(ij) [h(ij)/h(k)] \tag{7a}$$

$$Q(ij) = \left\{ \sum_k \Delta E'(ij \rightarrow k) [q(k)/Q(k)] \right\} q(ij). \tag{7b}$$

As shown by (5)–(7), CD is essentially a method to distribute ECoN and is thus characteristic of the geometry of each coordination polyhedron.

By comparing (1)–(2) with (5)–(7), the main differences between BV and CD methods can be summarized as follows.

(i) The computation performed by the BV method depends upon $q(ij)$ through the parameters of the *R-s*

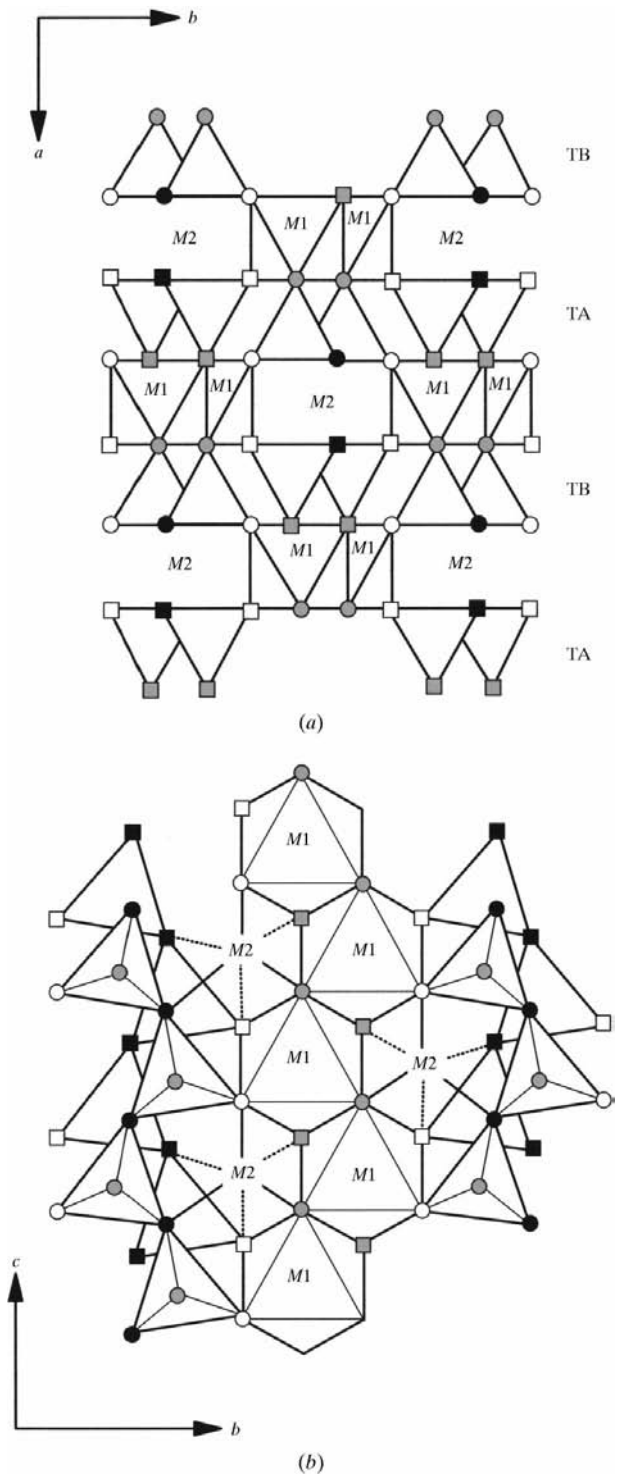

Fig. 1. (*a*) Schematic view along the *c* axis of the structure of orthopyroxenes, showing tetrahedral (TA and TB) and cation sites (*M*1 and *M*2). Circles: O atoms of the *B* chain; squares: O atoms of the *A* chain (see text). Grey: O1; white: O2; black: O3. (*b*) Projection along the *a* axis of part of the orthopyroxene structure. The edge (O2—O3) is shared between *M*2 and TA. Symbols are the same as in (*a*).

curve, although $q(ij)$ does not explicitly appear in (1). Instead, in the CD method $q(ij)$ is explicitly used as an input variable [see (5)–(7)], but the computation procedure does not depend on $q(ij)$, which plays the role of a multiplication factor of ECoN. In this sense, the bond weight $w(ij \rightarrow k)_l$ in the CD method [(5)] plays the role of the bond strength $s(ij \rightarrow k)_l$ [(1)] in the BV method.

(ii) The BV method *calculates* $Q(k)$ and $Q(ij)$ from the bond distances, and the parameters of the *R*-*s* curves depend upon the cations in each site, but are independent from the geometry of the specific site. On the other hand, in the CD method $Q(k)$ and $Q(ij)$ are the results of the *distribution* of $q(k)$ and $q(ij)$ as a function of ECoN in each polyhedron.

(iii) The contribution of each bond distance is scaled to an empirical parameter (the *normalizing parameter*) in the BV method, but to the shortest bond length in each polyhedron in the CD method.

(iv) Since the parameters used in the BV method depend upon the cation–anion pair, the computed BV changes in the presence of cation substitutions. On the other hand, since the CD method depends only upon the geometry of the coordination polyhedron, no difference is obtained by substituting cations with the same $q(ij)$ if the geometry of the polyhedron does not change.

(v) In the BV method $Q(k)$ and $Q(ij)$ are defined in the same way [(2*a*)–(2*b*)] and the ratios $q(k)/Q(k)$ and $q(ij)/Q(ij)$ closer to 1 are taken as an indication of a 'well performed' structure. In principle, a deviation of $q(k)/Q(k)$ and $q(ij)/Q(ij)$ from 1 may be due either to errors in the structure or to the presence of a real over- or under-bonding [hereinafter termed the OUB (Over–Under-Bonding) effect]. However, when the ratios $q(k)/Q(k)$ and $q(ij)/Q(ij)$ significantly differ from 1, it is difficult to distinguish the contribution from each of the above two causes. Instead, in the CD method $Q(ij)$ is a function of the ratio $q(k)/Q(k)$ and thus $Q(k)$ and $Q(ij)$ convey different information. In fact, (7*b*) shows that $Q(ij)$ represents the distribution of $q(k)/Q(k)$ among the cations [without the factor $q(k)/Q(k)$ (7*b*) would be just an identity $q(k) = Q(k)$, because the summation of $\Delta E'(ij \rightarrow k)$ is by definition 1]. Therefore, in the presence of OUB effects and without substantial errors in the structure, the charge (valence) unbalance on O atoms, which is measured by the $q(k)/Q(k)$ ratio, is distributed among all the cations bound to the *k*th oxygen, and the resulting $q(ij)/Q(ij)$ ratio should still be close to 1. In the CD method, $q(ij)/Q(ij)$ can thus be used to evaluate the correctness of the structure and $q(k)/Q(k)$ to investigate OUB, which depends on some real strain in the structure. In other words, when $q(ij)/Q(ij)$ is reasonably close to 1, $q(k)/Q(k)$ is a suitable parameter to investigate structural changes, *e.g.* as a function of composition, temperature and pressure. Obviously, a description in which anions are the centre

of the coordination polyhedra would invert the role of $Q(k)$ and $Q(ij)$.

3. Application of the CD method to pyroxenes

The choice of pyroxenes ($M2M1T_2O_6$; $M1$ and $M2$: extra-chain cations; T: tetrahedral cations) as a suitable test for the CD method was motivated by:

(i) the wide range of isomorphic substitutions in the M sites, which spans from Mg to In in the $M1$ site and from Li to Mn in the $M2$ site (Griffen, 1992);

(ii) the availability of reliable structural data for different structural types, which differ in the number of crystallographically independent silicate chains;

(iii) the availability of structural data on a wide range of temperature and pressure, at least for certain compositions.

For the purpose of the present research we have analysed orthopyroxenes (space group *Pbca*) and two types of clinopyroxenes (space groups $P2_1/c$ and $C2/c$), for which enough structure refinements have been reported. In orthopyroxenes and $P2_1/c$ clinopyroxenes two types of tetrahedral chains (TA and TB) exist, whereas $C2/c$ clinopyroxenes have only one.† With respect to the tetrahedral chains, apical O atoms are labelled O1, whereas basal O atoms are of two crystallographically independent types: O2 and O3. O3 are shared between pairs of tetrahedra and are thus termed 'bridging O atoms', whereas O2 are termed 'non-bridging O atoms'. The tetrahedral chains are parallel to bands of edge-sharing octahedra ($M1$), defined by O1 and O2. One oxygen of each type (O1, O2 and O3) from both chains (A and B) define a further site ($M2$), larger than $M1$ and with more irregular shape (Cameron & Papike, 1981). O3 is coordinated by the tetrahedral cations and by the cation in the $M2$ site, but not by the cation in the $M1$ site (Figs. 1*a* and *b*).

For $C2/c$ clinopyroxenes we have analysed only end-members, namely the three series of Ca, Na and Li pyroxenes. Solid solutions in $C2/c$ clinopyroxenes have not been included because they mostly involve light and heavy cations, in particular belonging to the two series Sc–Ti–V–Cr–Al and Mn–Fe–Ga–In, which show different correlations between structural and geometrical parameters (Ohashi *et al.*, 1990). For a given composition, structural changes with temperature and pressure are due mainly to the response of the metal–oxygen bonds to the changing conditions (Ohashi & Burnham, 1973), and the behaviour of the silicate chains is the result of those changes. Analysis of the variations in the chains thus permits the investigation of the correlation between applied conditions and structural changes.

In the literature, some analyses of the behaviour of the tetrahedral chains in pyroxenes have been reported. Baur (1971) compared four pairs of isostructural pyroxenes in terms of bond strength. Ferguson (1974) analysed the BV of eight clinopyroxenes and three orthopyroxenes. Sueno *et al.* (1976) analysed the Si—O and O3—O3—O3 angle variation *versus* temperature in orthoferrosilite. Takeda (1980) investigated the relation between Si—O distance and Si—O—Si angle in orthopyroxenes. Cameron & Papike (1981) analysed the variation of bond distances and bond angles on a large set of pyroxenes. Here we present the first analysis in terms of CD.

A set of 26 *Pbca* orthopyroxenes, nine $P2_1/c$ clinopyroxenes and 66 end-member $C2/c$ clinopyroxenes (Table 1), with accurate structural refinements, has been selected from the literature and on it BV (employing three different *R-s* curves: Brown & Shannon, 1973; Brown & Wu, 1976; Brown & Altermatt, 1985) and CD have been calculated.‡

The most suitable probe to investigate the variations in the T chains proved to be the computed charge of O3 [hereinafter labelled $Q(\mathrm{O3})$] as a function of the average $\langle d_{\mathrm{br}} \rangle$ of the two independent Si—O3 distances. $Q(\mathrm{O3})$ turns out to be particularly suitable because O3, differently from O1 and O2, is shared with the $M2$ site, but not with the $M1$ site. $Q(\mathrm{O3})$ is thus influenced by the presence of two cations, instead of three, as for the other two O atoms. The bond distance has been chosen as the independent variable rather than the O3—O3—O3 or Si—O3—Si angles used by previous researchers, because the CD method is based on a polyhedral description of the structure, in which the dependent variables, such as ECoN and Q, are defined in terms of bond distances, their relation with the angles being only indirect. For the sake of comparison, however, the Si—O3—Si angle is given henceforth as a function of the bond distances for the $C2/c$ clinopyroxenes, whereas for orthopyroxenes the corresponding analysis can be found in Takeda (1980).

Two 'variation parameters' are used henceforth: δ, which indicates the variation of the Si—O3—Si angle *versus* $\langle d_{\mathrm{br}} \rangle$, and ρ, for the $Q(\mathrm{O3})$ *versus* $\langle d_{\mathrm{br}} \rangle$ variation. δ^+ and δ^- on one hand, and ρ^+ and ρ^- on the other hand represent direct and inverse correlation change with $\langle d_{\mathrm{br}} \rangle$, respectively.

3.1. *Orthopyroxenes and $P2_1/c$ clinopyroxenes*

In these pyroxenes chain B is more kinked than chain A. TA tetrahedron shares one edge with the $M2$ site and is less distorted and smaller than TB, which does not share edges (Sueno *et al.*, 1976; Cameron & Papike, 1981). Al, when present, takes place in TB (Takeda,

† Pyroxenes with one or two types of tetrahedral chains are termed 'high pyroxenes' and 'low pyroxenes', respectively, in the OD theory (Sedlacek *et al.*, 1979).

‡ Supplementary data for this paper are available from the IUCr electronic archives (Reference: NA0093). Services for accessing these data are described at the back of the journal.

Table 1. *Structures used for BV and CD computations*

Samples 1–26 are *Pbca* orthopyroxenes; samples 27–35 are $P2_1/c$ clinopyroxenes; samples 36–101 are $C2/c$ clinopyroxenes.

No.	Formula	Ref.	No.	Formula	Ref.	No.	Formula	Ref.
1	$Co_2Si_2O_6$	(*a*)	35	$Fe_2Si_2O_6$	(*k*)	69	$NaAlSi_2O_6$ (2)	(*m*)
2	$Fe_2Si_2O_6$	(*a*)	36	$CaCoSi_2O_6$	(*l*)	70	$NaAlSi_2O_6$ 673 K	(*m*)
3	$Fe_2Si_2O_6$ 297 K	(*b*)	37	$CaFeSi_2O_6$ 297 K	(*m*)	71	$NaAlSi_2O_6$ 873 K	(*m*)
4	$Fe_2Si_2O_6$ 673 K	(*b*)	38	$CaFeSi_2O_6$ 673 K	(*m*)	72	$NaAlSi_2O_6$ 1073 K	(*m*)
5	$Fe_2Si_2O_6$ 783 K	(*b*)	39	$CaFeSi_2O_6$ 873 K	(*m*)	73	$NaCrSi_2O_6$	(*o*)
6	$Fe_2Si_2O_6$ 1073 K	(*b*)	40	$CaFeSi_2O_6$ 1073 K	(*m*)	74	$NaCrSi_2O_6$ 673 K	(*m*)
7	$Fe_2Si_2O_6$ 1173 K	(*b*)	41	$CaFeSi_2O_6$ 1173 K	(*m*)	75	$NaCrSi_2O_6$ 873 K	(*m*)
8	$Fe_2Si_2O_6$ 1253 K	(*b*)	42	$CaFeSi_2O_6$ 1273 K	(*m*)	76	$NaFeSi_2O_6$	(*o*)
9	$(FeMgCa)_2Si_2O_6$ 293 K	(*c*)	43	$CaFeSi_2O_6$ 0 GPa	(*n*)	77	$NaFeSi_2O_6$ 673 K	(*m*)
10	$(FeMgCa)_2Si_2O_6$ 448 K	(*c*)	44	$CaFeSi_2O_6$ 1.1 GPa	(*n*)	78	$NaFeSi_2O_6$ 873 K	(*m*)
11	$(FeMgCa)_2Si_2O_6$ 553 K	(*c*)	45	$CaFeSi_2O_6$ 2.1 GPa	(*n*)	79	$NaGaSi_2O_6$ (1)	(*t*)
12	$(FeMgCa)_2Si_2O_6$ 773 K	(*c*)	46	$CaFeSi_2O_6$ 2.8 GPa	(*n*)	80	$NaGaSi_2O_6$ (2)	(*u*)
13	$(FeMgCa)_2Si_2O_6$ 973 K	(*c*)	47	$CaFeSi_2O_6$ 3.6 GPa	(*n*)	81	$NaMnSi_2O_6$ (1)	(*v*)
14	$(FeMgCa)_2Si_2O_6$ 1123 K	(*c*)	48	$CaFeSi_2O_6$ 4.2 GPa	(*n*)	82	$NaScSi_2O_6$ (1)	(*w*)
15	$(FeMgCa)_2Si_2O_6$ 773 → 293 K	(*c*)	49	$CaFeSi_2O_6$ 4.6 GPa	(*n*)	83	$NaScSi_2O_6$ (2)	(*x*)
16	$Mg_2Si_2O_6$	(*a*)	50	$CaFeSi_2O_6$ 5.3 GPa	(*n*)	84	$NaTiSi_2O_6$ (1)	(*y*)
17	$Mg_2Si_2O_6$ 0 GPa	(*d*)	51	$CaFeSi_2O_6$ 6.3 GPa	(*n*)	85	$NaTiSi_2O_6$ (2)	(*z*)
18	$Mg_2Si_2O_6$ 1.04 GPa	(*d*)	52	$CaFeSi_2O_6$ 7.6 GPa	(*n*)	86	$NaVSi_2O_6$	(*aa*)
19	$Mg_2Si_2O_6$ 1.95 GPa	(*d*)	53	$CaFeSi_2O_6$ 8.7 GPa	(*n*)	87	$NaInSi_2O_6$ (1)	(*ab*)
20	$Mg_2Si_2O_6$ 3.27 GPa	(*d*)	54	$CaFeSi_2O_6$ 9.9 GPa	(*n*)	88	$NaInSi_2O_6$ (2)	(*ac*)
21	$Mg_2Si_2O_6$ 4.09 GPa	(*d*)	55	$CaMgSi_2O_6$	(*o*)	89	$NaInSi_2O_6$ (3)	(*ad*)
22	$Mg_2Si_2O_6$ 4.95 GPa	(*d*)	56	$CaMgSi_2O_6$ 673 K	(*m*)	90	$LiAlSi_2O_6$	(*o*)
23	$Mg_2Si_2O_6$ 5.85 GPa	(*d*)	57	$CaMgSi_2O_6$ 973 K	(*m*)	91	$LiAlSi_2O_6$ 572 K	(*m*)
24	$Mg_2Si_2O_6$ 7.00 GPa	(*d*)	58	$CaMgSi_2O_6$ 1123 K	(*m*)	92	$LiAlSi_2O_6$ 733 K	(*m*)
25	$Mg_2Si_2O_6$ 8.10 GPa	(*d*)	59	$CaMgSi_2O_6$ 1283 K	(*m*)	93	$LiAlSi_2O_6$ 1033 K	(*m*)
26	$Zn_2Si_2O_6$	(*e*)	60	$CaMgSi_2O_6$ 1 atm	(*p*)	94	$LiGaSi_2O_6$	(*ae*)
27	$(Mg_{0.31}Fe_{0.67}Ca_{0.015})_2Si_2O_6$ 293 K	(*f*)	61	$CaMgSi_2O_6$ 23.6 kbar	(*p*)	95	$LiGaSi_2O_6$	(*af*)
28	$(Mg_{0.31}Fe_{0.67}Ca_{0.015})_2Si_2O_6$ 473 K	(*f*)	62	$CaMgSi_2O_6$ 35.2 kbar	(*p*)	96	$LiGaSi_2O_6$	(*af*)
29	$(Mg_{0.31}Fe_{0.67}Ca_{0.015})_2Si_2O_6$ 673 K	(*f*)	63	$CaMgSi_2O_6$ 45.5 kbar	(*p*)	97	$LiGaSi_2O_6$	(*af*)
30	$(Mg_{0.31}Fe_{0.67}Ca_{0.015})_2Si_2O_6$ 873 K	(*f*)	64	$CaMgSi_2O_6$ 53.0 kbar	(*p*)	98	$LiFeSi_2O_6$	(*o*)
31	$(MgCr)_2Si_2O_6$	(*g*)	65	$CaNiSi_2O_6$	(*l*)	99	$LiVSi_2O_6$	(*ag*)
32	$Mn_2Si_2O_6$	(*h*)	66	$CaZnSi_2O_6$	(*q*)	100	$LiScSi_2O_6$	(*ah*)
33	$(Mg_{0.39}Fe_{0.52}Ca_{0.09})_2Si_2O_6$	(*i*)	67	$CaMnSi_2O_6$	(*r*)	101	$LiInSi_2O_6$	(*ai*)
34	$Mg_2Si_2O_6$	(*j*)	68	$NaAlSi_2O_6$ (1)	(*s*)			

(*a*) Sasaki *et al.* (1982); (*b*) Sueno *et al.* (1976); (*c*) Smyth (1973); (*d*) Hugh-Jones & Angel (1994) [atomic coordinates after Hugh-Jones, personal communication]; (e) Morimoto *et al.* (1975); (*f*) Smyth (1974); (*g*) Angel *et al.* (1989); (*h*) Tokonami *et al.* (1979); (*i*) Brown *et al.* (1972); (*j*) Ohashi (1984); (*k*) Smyth (1969); (*l*) Ghose *et al.* (1987); (*m*) Cameron *et al.* (1973); (*n*) Zhang *et al.* (1997); (*o*) Clark *et al.* (1969); (*p*) Levien & Prewitt (1981); (*q*) Ohashi *et al.* (1996); (*r*) Freed & Peacor (1967); (*s*) Prewitt & Burnham (1966); (*t*) Ohashi *et al.* (1983); (*u*) Ohashi, Osawa & Sato (1995); (*v*) Ohashi *et al.* (1987); (*w*) Ohashi *et al.* (1994*a*); (*x*) Hawthorne & Grundy (1973); (*y*) Ohashi *et al.* (1982); (*z*) Ohashi (1999*b*); (*aa*) Ohashi *et al.* (1994*b*); (*ab*) Ohashi *et al.* (1990); (*ac*) Hawthorne & Grundy (1974); (*ad*) Christensen & Hazell (1967); (*ae*) Sato *et al.* (1994); (*af*) Ohashi, Osawa, Sato & Onoda (1995); (*ag*) Satto *et al.* (1997); (*ah*) Hawthorne & Grundy (1977); (*ai*) Grotepaß *et al.* (1983) [atomic coordinates after Behruzi, personal communication].

1972). Sasaki *et al.* (1982) reported a difference in the so-called *net atomic charges* (Sasaki *et al.*, 1980) for atoms belonging to the two independent chains in $Co_2Si_2O_6$ and, to a lesser extent, for $Mg_2Si_2O_6$. Sueno *et al.* (1976) showed a different trend for the two chains of $Fe_2Si_2O_6$ in the plot of O3—O3—O3 *versus* temperature. There are thus evident differences between the two chains, which however were not revealed either by a bond strength analysis (Baur, 1971) or by a Si—O3—Si angle *versus* $\langle d_{br} \rangle$ plot (*angle plot*, henceforth; Takeda, 1980).

We have performed an analysis of the two chains for orthopyroxenes (Figs. 2 and 3) and for $P2_1/c$ clinopyroxenes (Figs. 4 and 5) in terms of Q(O3) *versus* $\Sigma Q = Q(O1) + Q(O2) + Q(O3)$ (Figs. 2 and 4) and of Q(O3) *versus* $\langle d_{br} \rangle$ (Q plot: Figs. 3 and 5). In the Q(O3) *versus* ΣQ plot (Figs. 2 and 4), it clearly appears that:

(i) the two chains are not completely balanced, as if $\Sigma QA = \Sigma QB = -6$, but with only one exception (see below), they occupy different regions, corresponding to $\Sigma QA < -6$ and $\Sigma QB > -6$;

(ii) data for chain *A* are scattered on a larger Q(O3) interval with respect to data for chain *B*.

For the reasons discussed below, some points are out of the trend: the points indicated as '*M*' ($Mg_2Si_2O_6$ measured at 7.0 GPa: Hugh-Jones & Angel, 1994) and '*Z*' ($Zn_2Si_2O_6$: Morimoto *et al.*, 1975) in Fig. 2, and the two points '*H*' (873 K refinement of hypersthene: Smyth, 1974) in Fig. 4.

Figs. 3 and 5 are the Q plots corresponding to Figs. 2 and 4. Points *M* and *Z* in Fig. 3 and points *H* in Fig. 5 have not been included in the regression lines (see §3.1.1). In Figs. 2–5 the two chains have different trends.

In particular, while the OUB effect appears for practically all the plotted pyroxenes, it is especially evident for O3B. This OUB effect is positively correlated with $\langle d_{br} \rangle$ (ρ^+) for chain *B*, whereas chain *A* shows a ρ^- correlation. The larger scatter for chain *A* in the *Q* plot corresponds to the similar larger scatter in the *Q versus* ΣQ plot (Fig. 2).

Further data, especially at high temperature (on the low $\langle d_{br} \rangle$ side), are desirable to confirm the trend in the corresponding region of the plot. The larger scatter appearing for chain *A* in Figs. 2–5 is likely due to the sharing of the O2—O3 edge between *M*2 and TA, which enhances the influence of the *M*2 cation on the TA site and reduces the rotation freedom of TA. Fig. 6(*a*) is the plot of the *M*2—O3*A* and *M*2—O3*B* distances against temperature for $Fe_2Si_2O_6$ and $(FeMgCa)_2Si_2O_6$; a similar plot is drawn against pressure in Fig. 6(*b*) for $Mg_2Si_2O_6$. The different slope of the *M*2—O3 regression line for the two chains is related to the geometrical constraint on O2*A*—O3*A* and the narrower range of *M*2—O3*A* may explain the narrower range of $\langle d_{br} \rangle$ values (Figs. 3 and 5), a fact that can partially hinder a clearer *Q*(O3) *versus* $\langle d_{br} \rangle$ correlation. The influence of *M*2 on TB, with which it shares only O3, is less relevant, and TB is not hindered from rotating around O2 in response to the variation of the applied conditions (temperature, pressure). The scatter of *Q*(O3*A*) is less evident in the case of $P2_1/c$ pyroxenes, which however represent fewer cations than orthopyroxenes.

3.1.1. *Remarks*. Baur (1971) stated that the dependence of the Si—O distance on the Si—O—Si angle is just a corollary of the more basic correlation between

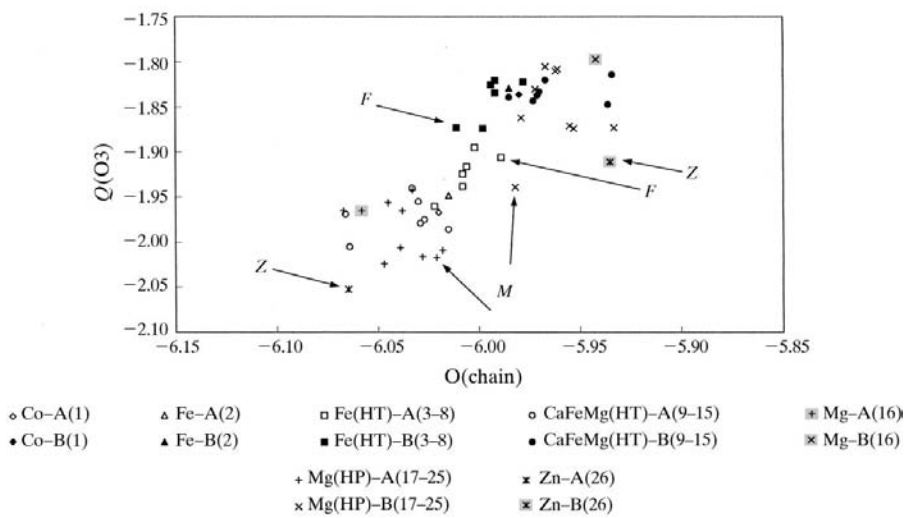

Fig. 2. *Q*(O3) *versus* ΣQ for orthopyroxenes (numbers in parentheses are the sample numbers, as given in Table 1). With a single exception (points F: $Fe_2Si_2O_6$ at 1173 K; data from Sueno *et al.*, 1976), the two chains occupy different regions, corresponding to $\Sigma QA < -6$ and $\Sigma QB > -6$. Points *M* ($Mg_2Si_2O_6$ at 7.0 GPa: Hugh-Jones & Angel, 1994) are considered anomalous (see Fig. 3). Data for chain *A* are dispersed on a larger interval of *Q*(O3), perhaps owing to the geometrical constraints arising from the O2—O3 edge sharing between *M*2 and TA.

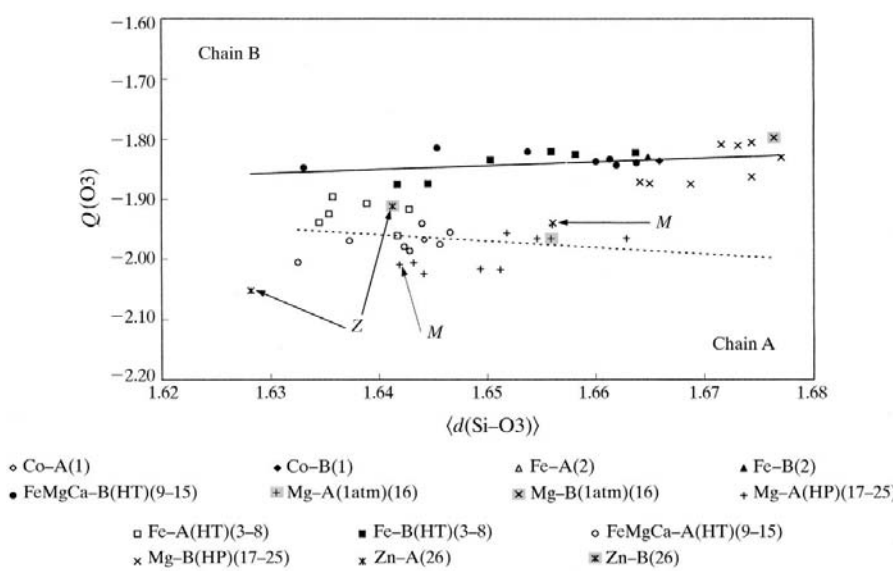

Fig. 3. *Q* plot [*Q*(O3) *versus* $\langle d_{br} \rangle$] for orthopyroxenes (numbers as given in Fig. 2). An opposite trend appears for the two chains (ρ^- for chain *A* and ρ^+ for chain *B*). Scattering of data for chain *A* is consistent with the similar effect seen in Fig. 2. Points *M* ($Mg_2Si_2O_6$ at 7.0 GPa: Hugh-Jones & Angel, 1994) and *Z* ($Zn_2Si_2O_6$: Morimoto *et al.*, 1975) are anomalous with respect to the general trend. The anomaly for point *M* regards chain *B* only (full-line arrow). Interpretation of the anomalies is given in the text.

the variation of bond length and the variation of bond strength. Takeda (1980) analysed the $Si-O_{br}-Si$ variations as a function of $\langle d_{br} \rangle$ and reported a δ^- (*i.e.* inverse) correlation for both chains. On the other hand, the Q plot (corresponding to the bond strength–distance correlation in Baur's approach) shows that the two chains have a different trend. The differences between the angle plot and the Q plot thus lead us to reconsider Baur's (1971) statement, which was likely based on approximations which were too drastic.

The Q plot is also able to discover anomalous structural data. The point M in Fig. 3 corresponds to the data of $Mg_2Si_2O_6$ (orthoenstatite) collected at 7.0 GPa (Hugh-Jones & Angel, 1994), for which the O1B and O3B x coordinates are out of the general trend *versus* pressure of the whole series (Fig. 7). The sample might have been measured at high pressure before it could reach the equilibrium state, thus preserving some memory of the ambient pressure structure. The points Z in Fig. 3 correspond to the orthorhombic $Zn_2Si_2O_6$ and the anomaly is perhaps related to structural differences at the synthesis and refinement pressures (see *Discussion*). The two points H (Figs. 4 and 5) correspond to hypersthene at 873 K. Their Q(O3B) significantly differ from the general trend shown by the other eight pyroxenes and the two chains are more unbalanced than

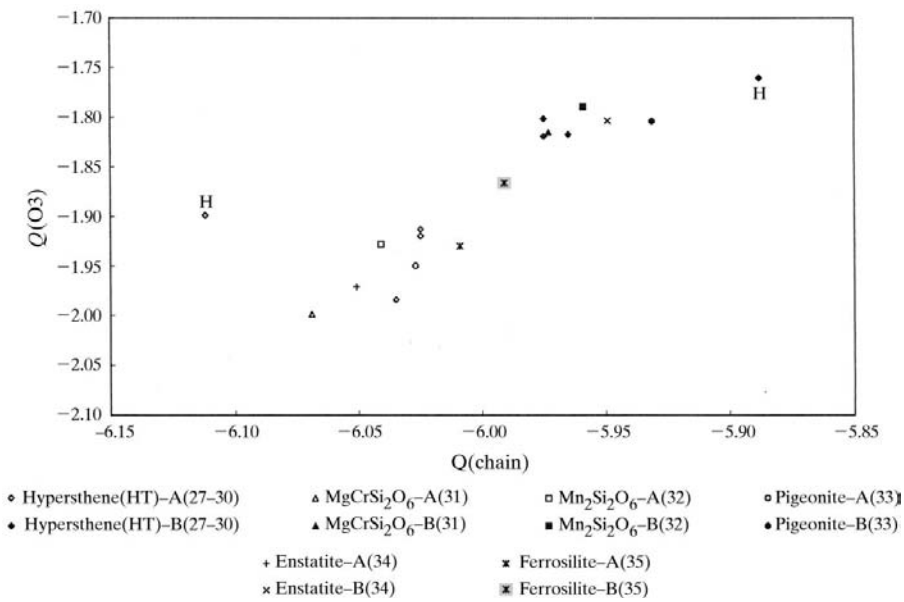

Fig. 4. Q(O3) *versus* ΣQ for $P2_1/c$ clinopyroxenes (numbers as in Fig. 2). Data for hypersthene at 873 K (indicated as H; data from Smyth, 1974) are outside the region in which all the other data, including those for orthopyroxenes (Fig. 2), are found.

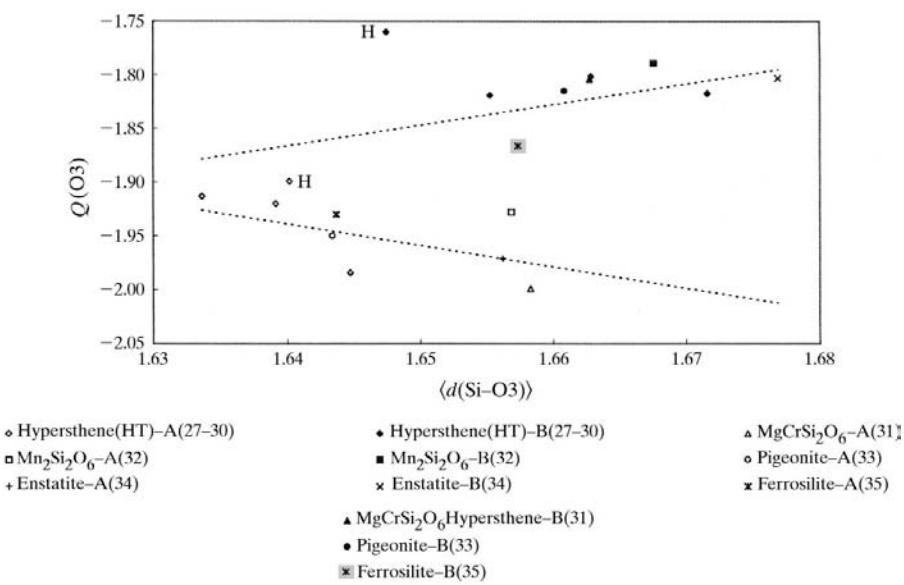

Fig. 5. Q plot for $P2_1/c$ clinopyroxenes (numbers as in Fig. 2). Chains B and A show a ρ^+ and ρ^- variation, respectively. Data at 873 K (indicated as H: Smyth, 1974) have not been included in the calculation of the regression line.

all the other cases (data for the same sample at 973 K have not been considered at all, because the published atomic coordinates and cell parameters do not match the bond distances).

3.2. *C2/c clinopyroxenes*

For the sake of comparison with the analysis performed for orthopyroxenes, both the Q plot and the angle plot are given (Figs. 8 and 9) for Ca, Na and Li end-members.

The angle plot (Fig. 8) shows δ^+ variation for all three series, although points for the Li series are better explained by dividing them in three different regions, as discussed below together with the reasons of excluding points for $CaMnSi_2O_6$ and for $NaInSi_2O_6$ from the regression lines of the respective series.

The Q plot (Figs. 9*a–c*) also shows a direct correlation (ρ^+). The following differences between the two plots need, however, to be considered:

(i) data for Ca pyroxenes follow the same trend in the angle plot, whereas in the Q plot they split;

(ii) for $CaMgSi_2O_6$ (diopside) both temperature and pressure variations (ΔT and Δp) produce an almost continuous series of data in both plots; on the other hand, for $CaFeSi_2O_6$ (hedenbergite) the ΔT and Δp data show a different trend, although the latter are more dispersed, especially in the Q plot;

(iii) data for $CaMnSi_2O_6$ (Freed & Peacor, 1967) and for one of the $NaInSi_2O_6$ samples (Christensen & Hazell, 1967) appear out of the trend in the angle plot (Fig. 8), but not in the Q plot (Figs. 9*a* and *b*).

The difference in the Q plot between $CaMgSi_2O_6$ and $CaFeSi_2O_6$ agrees well with the 'hard' and 'soft' core of Mg and Fe, respectively, and then the coordination polyhedra of Mg are less modified by pressure and temperature than those of Fe (Hazen & Finger, 1982).

Three refinements of $NaInSi_2O_6$ have been reported (Christensen & Hazell, 1967; Hawthorne & Grundy,

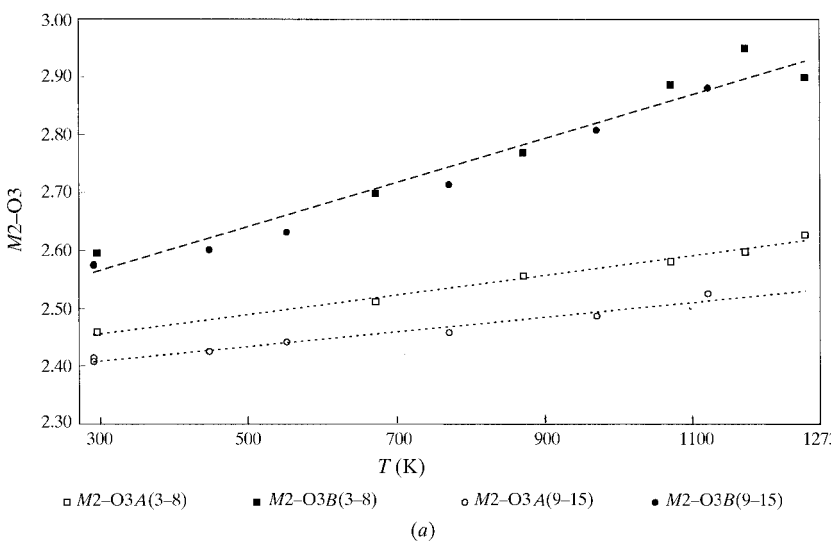

Fig. 6. $M2-O3$ distance *versus* temperature [(*a*) $Fe_2Si_2O_6$; samples 3–8 and $(FeMgCa)_2Si_2O_6$, samples 9–15] and *versus* pressure (*b*) $Mg_2Si_2O_6$; samples 17–25]. In both cases $M2-O3A$ and $M2-O3B$ have a different trend, which is likely owing to the sharing of an edge between the $M2$ octahedron and the TA tetrahedron. Data for $Fe_2Si_2O_6$ and $(FeMgCa)_2Si_2O_6$ are separated for chain A, but the trends are almost parallel.

1974; Ohashi *et al.*, 1990), one of which (Christensen & Hazell, 1967) is in certain respects anomalous. The latter sample was obtained under hydrothermal conditions as a byproduct in the synthesis of indium oxides and shows peculiar lattice parameters. The other two samples were instead synthesized at high temperature and in dry conditions [for the synthesis conditions of sample No. 88 refer to Ito (1968), especially p. 1666]. The sample of Christensen & Hazell (1967) appears out of the general trend in the angle plot (Fig. 8), but both the Q(O3) value and its position in the Q plot indicate no structural anomaly. The above differences thus reflect true structural differences owing to the different synthesis conditions, rather than imprecision of the structure refinement. A similar argument arises from the comparison of the angle plot (Fig. 8) and the Q plot (Fig. 9*a*) for $CaMnSi_2O_6$ (Freed & Peacor, 1967), for which the point in the Q plot is more or less on the prolongation of the regression line for Ca pyroxenes towards long $\langle d_{br} \rangle$ values.

Data for Li pyroxenes have a strictly similar trend in both the angle plot (Fig. 8) and the Q plot (Fig. 9c), but appear divided into three regions. $LiAlSi_2O_6$ (spodumene) is far from the data for the other Li pyroxenes and a second slope change appears in the correspondence of $LiScSi_2O_6$. Differently from other cations, the coordination of Li is generally controlled by the arrangement of more rigid groups (Ferraris *et al.*, 1999), and Li—O bonds are well described by a soft-sphere model (Wenger & Armbruster, 1991). These characteristics of Li are reflected by the plot of the Li—O distance *versus* ECoN (Fig. 10), where the different compounds show peculiar behaviour.

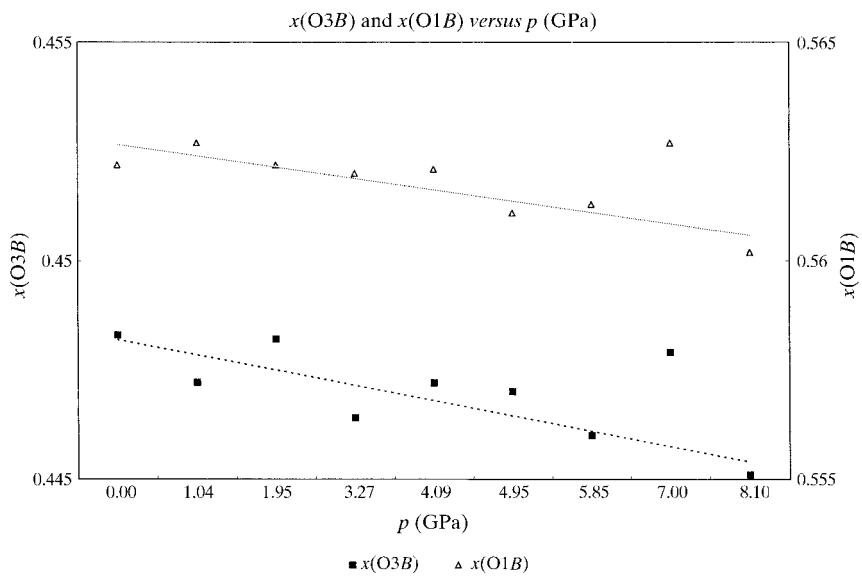

Fig. 7. x coordinate of O1*B* (white triangles) and O3*B* (black squares) *versus* pressure for $Mg_2Si_2O_6$ (samples 17–25 of Table 1). The x coordinates at 7.0 GPa significantly differ from the general trend, showing that the sample measured at that pressure had probably not reached the equilibrium, but was still keeping a memory of the room-pressure structure.

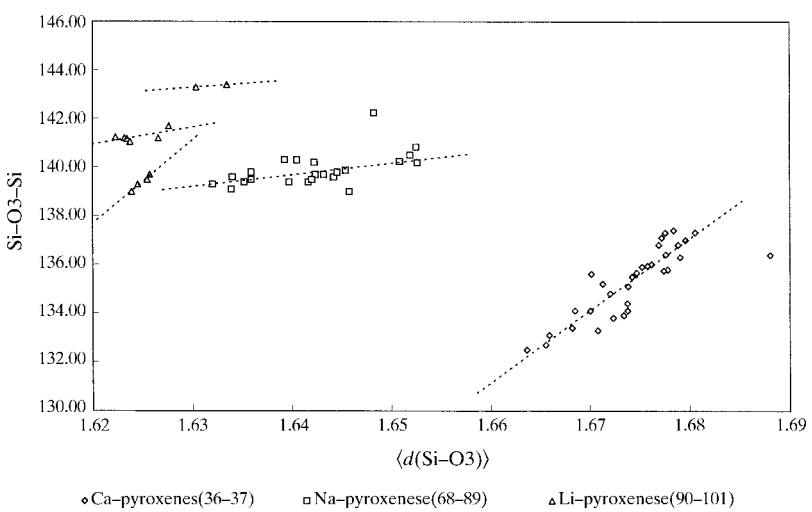

Fig. 8. Angle plot for Ca, Na and Li end-member *C*2/*c* clinopyroxenes (numbers as in Fig. 2). Data indicated by an arrow seem anomalous, but they are rationalized in the Q plot (Figs. 9*a* and *b*).

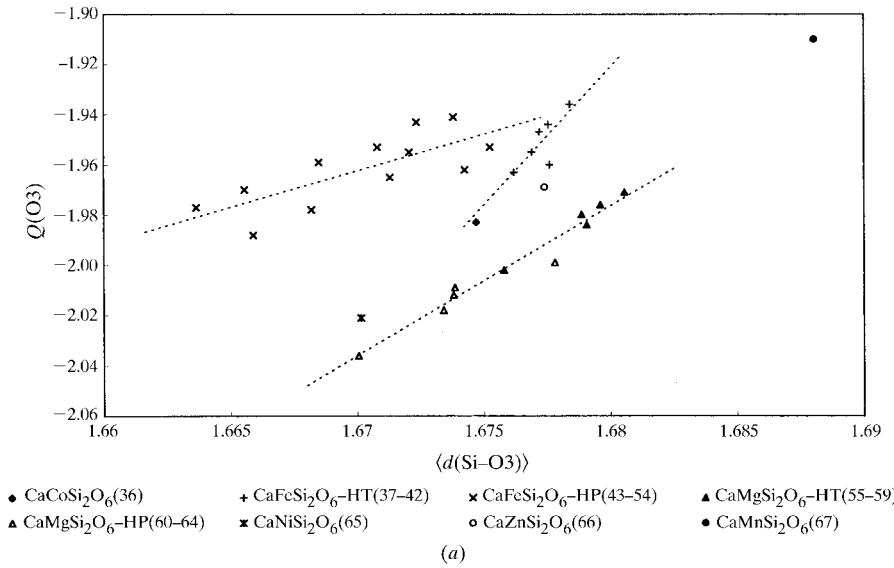

◆ $CaCoSi_2O_6$(36) + $CaFeSi_2O_6$–HT(37–42) × $CaFeSi_2O_6$–HP(43–54) ▲ $CaMgSi_2O_6$–HT(55–59)
▲ $CaMgSi_2O_6$–HP(60–64) ⧗ $CaNiSi_2O_6$(65) ○ $CaZnSi_2O_6$(66) ● $CaMnSi_2O_6$(67)

(*a*)

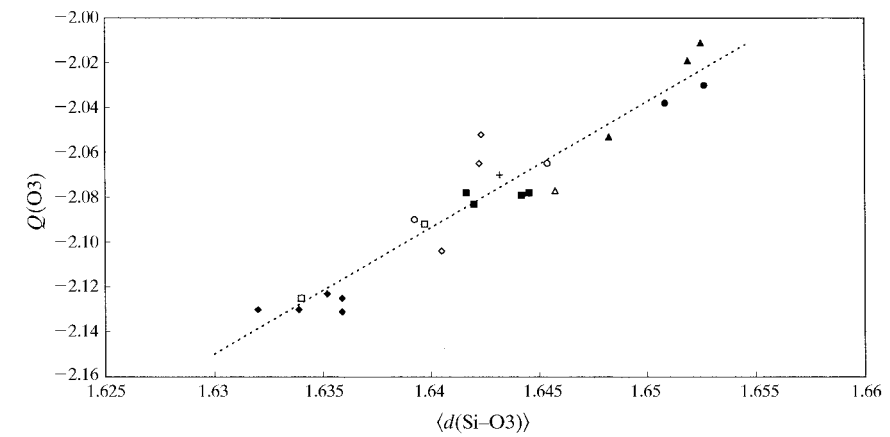

◆ $NaAlSi_2O_6$(68–72) ◇ $NaCrSi_2O_6$(73–75) ■ $NaFeSi_2O_6$(76–78) □ $NaGaSi_2O_6$(79–80) △ $NaMnSi_2O_6$(81)
● $NaScSi_2O_6$(82–83) ○ $NaTiSi_2O_6$(84–85) + $NaVSi_2O_6$(86) ▲ $NaInSi_2O_6$(87–89)

(*b*)

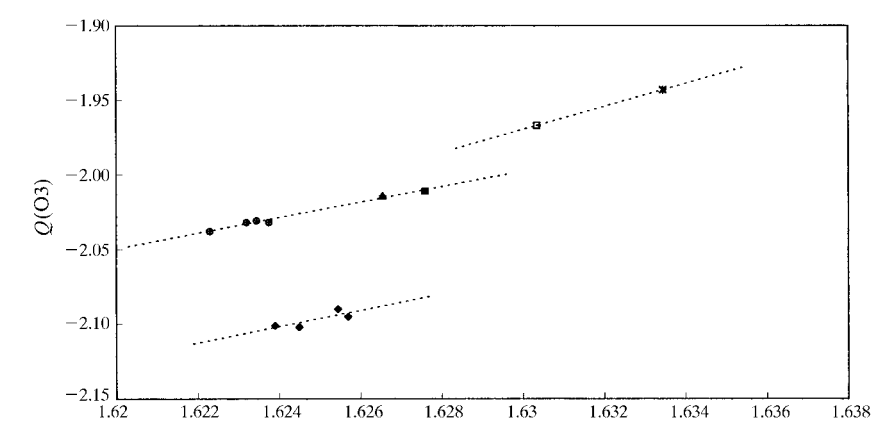

◆ $LiAlSi_2O_6$(90–93) ○ $LiGaAl_2SiO_6$(94–97) ▲ $LiFeSi_2O_6$(98)
■ $LiVSi_2O_6$(99) ⧗ $LiScSi_2O_6$(100) □ $LiInSi_2O_6$(101)

(*c*)

Fig. 9. *Q* plot for (*a*) Ca, (*b*) Na and (*c*) Li *C*2/*c* clinopyroxenes. Data for Ca pyroxenes are well separated in the *Q* plot, whereas they are practically overlapped in the angle plot (Fig. 8). The value corresponding to the $NaInSi_2O_6$ hydrothermal sample (Christensen & Hazell, 1967) and for $CaMnSi_2O_6$ (Freed & Peacor, 1967) are completely outside the region occupied by the other structures, but they are instead perfectly normal in the *Q* plot. Three different zones appear for Li pyroxenes, namely $LiAlSi_2O_6$, $Li(Ga,Fe,V,Ti)Si_2O_6$ and $Li(Sc,In)Si_2O_6$. These three regions are rationalized in terms of Li coordination (Fig. 10). Numbers as in Fig. 2.

4. Discussion

The CD method was introduced by Hoppe *et al.* (1989) mainly as an alternative tool to the BV method to distribute bond strength. It basically differs from the BV method in the use of only experimental bond distances in each coordination polyhedron, without any empirical normalizing parameter. Besides, since the empirical parameters used by BV were derived at ambient pressure and temperature, the BV method is especially thought to deal with structures in those conditions. The CD method does not suffer from such a limitation.

Hoppe *et al.* (1989) demonstrated that better results are obtained from CD on oxide compounds; this can be shown by the q/Q ratio. The present research has proved that such criterion can be used only in the absence of OUB effects and that the results of the calculation, namely $Q(k)$ and $Q(ij)$, have a different meaning in the CD and in the BV methods. In particular, $Q(k)$ and $Q(ij)$ computed according to CD permit to separately assess the correctness of the structure [$Q(ij)$] and to investigate the dependence of the structural details from composition, temperature and pressure [$Q(k)$]. An application of ECoN was previously reported by Weiss *et al.* (1992), who proved the existence of a correlation between the ECoN of the interlayer cation and the amount of tetrahedral rotation angle in phyllosilicates.

The BV method deals with coordination polyhedra of a given cation–anion pair in the same way in any structure, whereas the CD method treats each coordination polyhedron independently. It follows that any change (even at constant volume) of a given coordination polyhedron modifying the shortest bond length of the polyhedron is scaled in a different way, whereas in the BV method the same normalizing parameter is always used.

Gibbs *et al.* (1998) related the strength of a bond $s(ij \rightarrow k)_l$ [(1)] to the electron density along it and to the electronegativity of the cation. As mentioned above, in the CD method the bond weight $w(ij \rightarrow k)_l$ [(5)] plays the role of the bond strength $s(ij \rightarrow k)_l$ [(1)], but it is defined in a more geometrical way, in terms of the coordination polyhedra. The cation–anion pair does not explicitly enter in the definition of the bond weight, as it does in the case of the bond strength through the empirical parameters, but it determines the bond distances in terms of which the bond weight is defined. A correlation similar to that reported by Gibbs *et al.* (1998) for the bond strength may thus probably also exist for the bond weight.

4.1. *CD analysis of $CaFeSi_2O_6$*

Zhang & Hafner (1994) analysed a series of $CaFeSi_2O_6$ pyroxenes at different pressure and reported a discontinuity in the Mössbauer spectrum at ~4 GPa. Zhang *et al.* (1997) refined the X-ray crystal structure of the sample previously analysed by Zhang & Hafner (1994) up to 10 GPa, but could not reveal any discontinuity in the structure. Ohashi (1999*a*) re-examined their data and showed a small but significant discontinuity in the plot of Fe—Fe *versus* ⟨Fe—O1⟩ distances at ~6 GPa. A CD analysis gives the following insights.

Fig. 11*a* is the plot of ⟨Q(O1,O2)⟩ [mean value of Q(O1) and Q(O2)] *versus* pressure for the same series of $CaFeSi_2O_6$ pyroxene. ⟨Q(O1,O2)⟩ has been chosen because O1 and O2 are directly bound to Fe. A discontinuity appears at ~6 GPa, which is even more marked than the Fe—Fe discontinuity reported by Ohashi (1999*a*) at the same pressure. Such a discontinuity can be due to an increase with pressure of the repulsion between 3*d* non-bonding electrons of Fe and the O1 atoms, which finally modifies the octahedron geometry. A similar effect of the 3*d* electrons has already been reported in both Na and Ca pyroxenes: for members in which the *M*1 cation has 3*d* non-bonding electrons, the *M*1—*M*1 distances are shorter than those expected from the *M*1—O1 distances (Ohashi *et al.*,

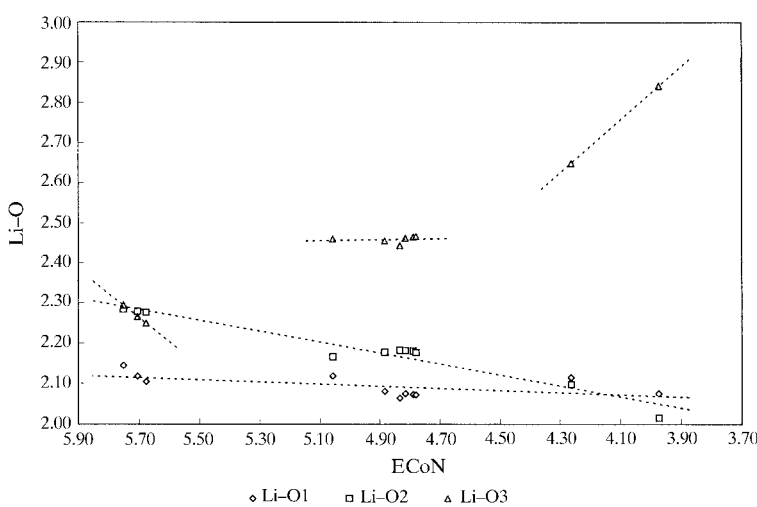

Fig. 10. Li—O distance *versus* ECoN. Data refer to samples 93, 91, 90, 98, 97, 99, 96, 94, 95, 100 and 101 (Table 1), respectively (decreasing ECoN sequence). Two transitions appear, producing the three regions shown in Fig. 8 (samples 93–98; 97–95; 100–101). These transitions are likely to be due to the fact that the coordination of Li is generally controlled by the arrangement of more rigid groups (Wenger & Armbruster, 1991; Ferraris *et al.*, 1999).

1987; Ohashi, 1988). The plot of the Quadratic Elongation (Robinson *et al.*, 1971) *versus* pressure (Fig. 11*b*) shows that this effect is related with a discontinuity in the octahedral distortion at ~6 GPa.

Fig. 11*c* is the plot of ECoN for the Fe coordination polyhedron *versus* pressure. In the region between 4 and 6 GPa a drastic variation appears, whereas in the two regions below and above it, the trend is almost flat. The

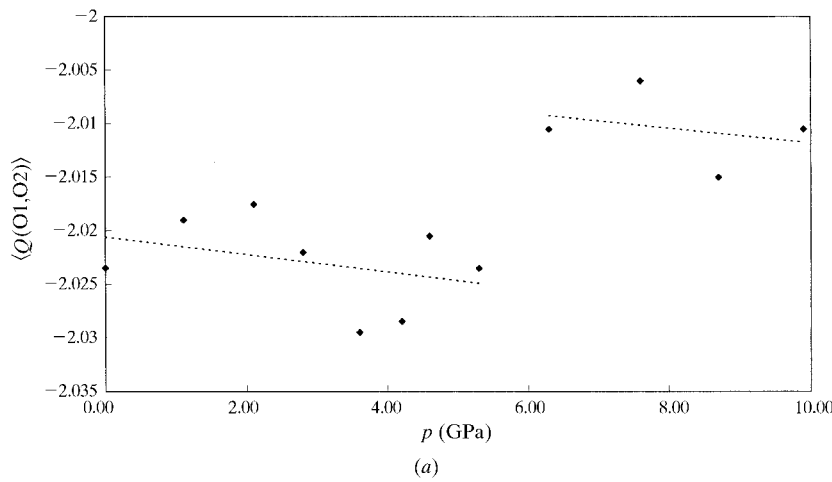

(*a*)

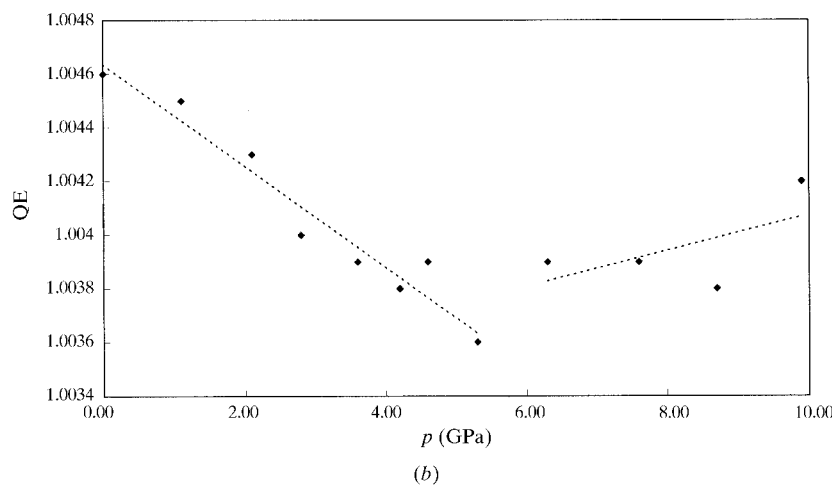

(*b*)

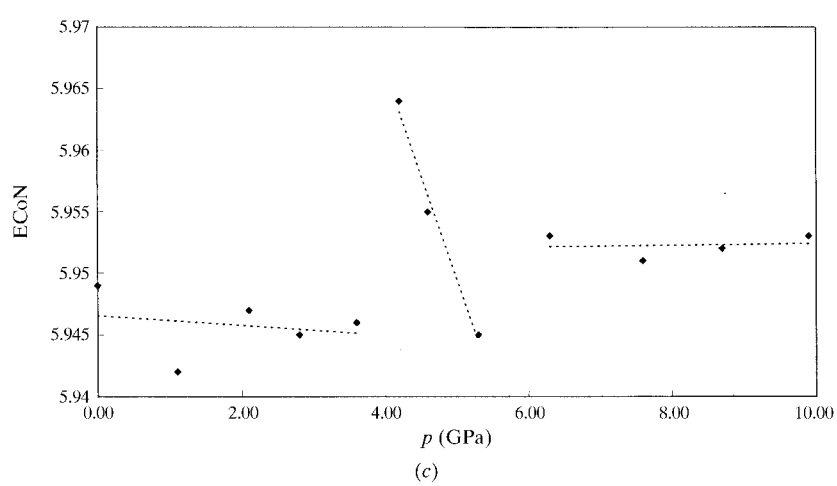

(*c*)

Fig. 11. (*a*) ⟨*Q*(O1,O2)⟩, (*b*) Quadratic Elongation (QE) and (*c*) ECoN *versus* pressure for $CaFeSi_2O_6$ (samples 43–54 in Table 1: Zhang *et al.*, 1997). Figs. 11*a* and *b* show a discontinuity at ~6 GPa, which is perhaps due to a repulsion between 3*d* non-bonding electrons and O1 atoms (Ohashi *et al.*, 1987; Ohashi, 1988), which modifies the geometry of the octahedron and shortens the Fe—Fe distances. Fig. 11(*c*) shows two discontinuities: one is located at ~6 GPa and confirms the other two plots, the second appears at ~4 GPa and confirms the discontinuity in the Mössbauer spectrum reported by Zhang & Hafner (1994).

two discontinuities, in the Mössbaeur spectrum and in the geometrical parameters [Fe—Fe distance; ⟨*Q*(O1,O2)⟩; quadratic elongation], likely appear corresponding to the two values for which the Fe coordination undergoes the most relevant changes.

4.2. *CD analysis of orthorhombic $Zn_2Si_2O_6$*

Morimoto *et al.* (1975) refined the quenched structures of both *C*2/*c* and *Pbca* $Zn_2Si_2O_6$ pyroxenes, showing that, differently from the Fe and Mg end-members, the two polymorphs are not in a cell–twin (Ito, 1935, 1950) relation. Both polymorphs are not stable at room temperature and pressure (Syono *et al.*, 1971; Olesch *et al.*, 1982; Kudoh *et al.*, 1989).

In the *C*2/*c* polymorph quenched from 1673 K and 70 kbar, Zn in the *M*2 site is only tetrahedrally coordinated by O atoms. Kudoh *et al.* (1989) reported a discontinuity for the monoclinic polymorph at 5.1 GPa in the cell volume and in the compressibility, showing the existence of a phase transition. The low-pressure *C*2/*c* $Zn_2Si_2O_6$ is thus not isostructural with high-pressure $Zn_2Si_2O_6$: the coordination of Zn in the *M*2 site for the latter is not known.

Syono *et al.* (1971), in a study of the high-pressure transformations in zinc silicates, obtained orthorhombic $Zn_2Si_2O_6$ as a by-product during the synthesis of Zn_2SiO_4. They stated that orthorhombic $Zn_2Si_2O_6$ has no stability field in the phase diagram, but later Olesch *et al.* (1982) suggested it may exist as a stable phase at high temperature and pressure. Morimoto *et al.* (1975) refined an orthorhombic $Zn_2Si_2O_6$, after quenching the crystal from 1673 K and 8.4 GPa. An investigation into the possible phase transition, similar to that by Kudoh *et al.* (1989) for the monoclinic polymorph, has not been attempted. However, the relation between the cell volume and the ionic radius (Shannon & Prewitt, 1970) of the cation in the *M*2 site (Fig. 12) shows that orthorhombic $Zn_2Si_2O_6$ has an unusually large cell volume in comparison with other orthopyroxenes. Besides, differently from other pyroxenes, the cell volume is also influenced by the synthesis conditions (Olesch *et al.*, 1982). It is thus reasonable to suspect that a phase transition occurs similar to that of the monoclinic polymorph and that the sample measured at ambient conditions is not isostructural with the product of the synthesis. In the quenched sample studied by Morimoto *et al.* (1975), within a distance of less than 3.0 Å, Zn in the *M*2 site has six O atoms, which however are arranged in a 4 + 2 coordination with long *M*2—O3 bonds, typical of *Pbca* orthopyroxenes (Domeneghetti *et al.*, 1985). The CD analysis (Table 2) reveals that, differently from other *Pbca* orthopyroxenes, the contribution by O3 to ECoN [(4)–(6)] is negligible, and

Table 2. *ECoN and CD for monoclinic and orthorhombic $Zn_2Si_2O_6$ (Morimoto et al., 1975)*

	Atom	*q*	ECoN	*Q*	*q*/*Q*
Pbca $Zn_2Si_2O_6$	Zn1	2	5.361	1.961	1.020
	Zn2	2	3.899	1.967	1.017
	Si1	4	3.996	4.032	1.001
	Si2	4	3.987	4.04	1.003
				σ = 0.042	
	O1*A*	−2		−2.067	0.968
	O1*B*	−2		−1.98	1.010
	O2*A*	−2		−1.946	1.028
	O2*B*	−2		−2.045	0.978
	O3*A*	−2		−2.052	0.975
	O3*B*	−2		−1.911	1.047
				σ = 0.064	
*C*2/*c* $Zn_2Si_2O_6$	Zn1	2	5.117	1.97	1.015
	Zn2	2	3.906	1.973	1.014
	Si	4	3.996	4.028	1.001
				σ = 0.035	
	O1	−2		−2.038	0.981
	O2	−2		−2.019	0.991
	O3	−2		−1.943	1.030
				σ = 0.05	

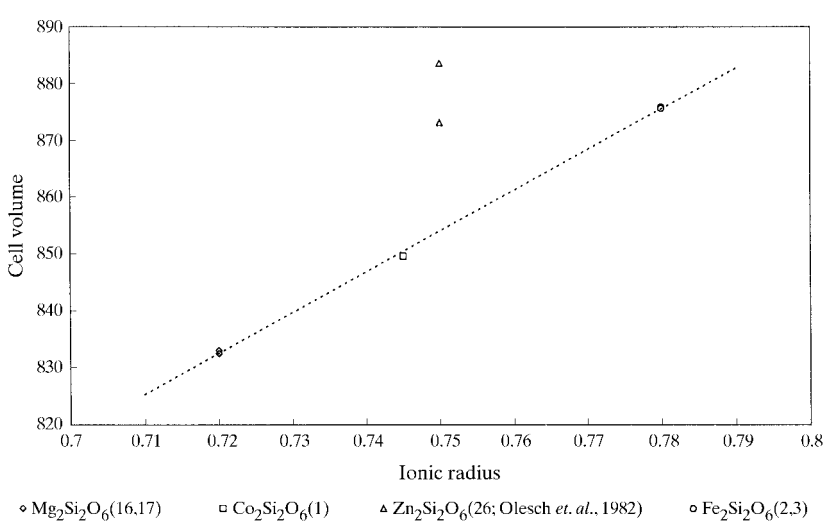

Fig. 12. Cell volume *versus* ionic radius for seven orthopyroxene samples. The Zn end-member has an unusually large cell volume. The two values for $Zn_2Si_2O_6$ are rather different and depend upon the synthesis conditions. On the other hand, pairs of values for $Mg_2Si_2O_6$ and $Fe_2Si_2O_6$ are practically overlapped.

ECoN of Zn in the *M*2 site is practically the same in the two polymorphs studied by Morimoto *et al.* (1975), namely slightly lower than four (Table 2). It follows that in both polymorphs O3 is practically not bonded to Zn in the *M*2 site.

With a q(O3)/Q(O3) ratio close to 1 for both chains, almost no OUB effect appears in the orthorhombic $Zn_2Si_2O_6$ and the points representing it in the Q plot (points Z in Fig. 3) occupy an anomalous position with respect to the other orthopyroxenes. The separation of Q(O3B) from the regression line for chain B is more or less the same as the separation of Q(O3A) from the regression line for chain A and it can be considered as a measure of the OUB effect that would be present if O3B were bonded to *M*2, as it is for the other orthopyroxenes. The absence of the OUB effect appears not directly related to the thermodynamic stability: in fact, the orthorhombic low-pressure $Zn_2Si_2O_6$, for which the OUB effect is practically absent, has no stability field, the stable phases being willemite and quartz (Syono *et al.*, 1971; Olesch *et al.*, 1982). From the anomalous position in the Q plot (Fig. 3), the opposite might be rather inferred: a certain OUB effect seems to be invariably present in the structure of orthopyroxenes.

5. Conclusions

It has been shown that the CD method is a suitable alternative to BV to analyse the distribution of bond strength/bond valence. In particular, the different definition of $Q(ij)$ and $Q(k)$ permits the separate evaluation of the quality of the structure and the degree of the OUB effect.

The two crystallographically independent tetrahedral chains of orthopyroxenes and $P2_1/c$ clinopyroxenes are characterized by different ΣQ values, and Q(O3) for the two chains has a different dependence with $\langle d_{\rm br}\rangle$. The CD analysis thus confirms the difference in the two chains previously revealed, although with some uncertainties, by means of geometrical parameters (Sueno *et al.*, 1976) or measured electron density (Sasaki *et al.*, 1982).

The CD analysis is a suitable tool to check the presence of structural anomalies, as shown by the examples $CaMnSi_2O_6$, $NaInSi_2O_6$ and the $Mg_2Si_2O_6$ orthopyroxene at 7.0 GPa. The anomalous position in the Q plot for orthorhombic $Zn_2Si_2O_6$ is due to an unusual coordination for the *M*2 site and suggests the existence of differences between the refined structure and the structure under the conditions of the synthesis.

The relation between Q(O3) and the experimental bond lengths gives a simple and handy correlation between structural changes, on one hand, and the composition with the experimental conditions, on the other hand; the quality of the structure refinement is an important prerequisite.

This research has been developed during a post-doctoral program (MN) supported by the Japanese Science and Technology Corporation. GF acknowledges the Italian National Research Council (CNR) and Ministry of University, and of Technology and Scientific Research (MURST) for financial support.

References

Allman, R. (1975). *Monatsh. Chem.* **106**, 779–793.
Angel, R. J., Gasparik, T. & Finger, L. W. (1989). *Am. Mineral.* **74**, 599–603.
Balić Žunić, T. & Makovicky, E. (1996). *Acta Cryst.* B**52**, 78–81.
Baur, W. H. (1970). *Trans. Am. Cryst. Ass.* **6**, 129–155.
Baur, W. H. (1971). *Am. Mineral.* **56**, 1573–1599.
Brown, G. E., Prewitt, C. T., Papike, J. J. & Sueno, S. (1972). *J. Geophys. Res.* **77**, 5778–5789.
Brown, I. D. (1977). *Acta Cryst.* B**33**, 1305–1310.
Brown, I. D. (1978). *Chem. Soc. Rev.* **7**, 359–376.
Brown, I. D. (1988). *Acta Cryst.* B**44**, 545–553.
Brown, I. D. & Altermatt, D. (1985). *Acta Cryst.* B**41**, 244–247.
Brown, I. D. & Shannon, R. D. (1973). *Acta Cryst.* A**29**, 266–282.
Brown, I. D. & Wu, K. K. (1976). *Acta Cryst.* B**32**, 1957–1959.
Cameron, M. & Papike, J. J. (1981). *Am. Mineral.* **66**, 1–50.
Cameron, M., Sueno, S., Prewitt, C. T. & Papike, L. L. (1973). *Am. Mineral.* **58**, 594–618.
Chiari, G. (1988). *Z. Kristallogr.* **185**, 504.
Chiari, G. (1990). *Acta Cryst.* B**46**, 717–723.
Christensen, A. N. & Hazell, R. G. (1967). *Acta Chem. Scand.* **21**, 1425–1429.
Clark, J. R., Appleman, D. E. & Papike, J. J. (1969). *Mineral. Soc. Am. Spec. Pap.* **2**, 31–50.
Domeneghetti, M. C., Molin, G. M. & Tazzoli, V. (1985). *Am. Mineral.* **70**, 987–995.
Donnay, G. & Allman, R. (1970). *Am. Mineral.* **55**, 1003–1015.
Ferguson, R. B. (1974). *Acta Cryst.* B**30**, 2527–2539.
Ferraris, G. & Catti, M. (1973). *Acta Cryst.* B**29**, 2006–2009.
Ferraris, G., Prencipe, M., Pautov, L. A. & Sokolova, E. V. (1999). *Can. Mineral.* **37**, 769–774.
Freed, R. L & Peacor, R. (1967). *Am. Mineral.* **52**, 709–720.
Ghose, S., Wan, C. & Okamura, F. P. (1987). *Am. Mineral.* **72**, 375–381.
Gibbs, G. V., Hill, F. C., Boisen, M. B. & Downs, R. T. (1998). *Phys. Chem. Miner.* **25**, 585–590.
Gopal, R. (1972). PhD Thesis. McMaster University.
Griffen, D. T. (1992). *Silicate Crystal Chemistry*. Oxford University Press.
Grotepaß, M., Behruzi, M. & Hahn, T. (1983). *Z. Kristallogr.* **162**, 90–91.
Hawthorne, F. C. & Grundy, H. D. (1973). *Acta Cryst.* B**29**, 2615–2616.
Hawthorne, F. C. & Grundy, H. D. (1974). *Acta Cryst.* B**30**, 1882–1884.
Hawthorne, F. C. & Grundy, H. D. (1977). *Can. Mineral.* **15**, 50–58.
Hazen, R. M. & Finger, L. W. (1982). *Comparative Crystal Chemistry: Temperature, Pressure, Composition and the Variation of Crystal Structure.* New York: Wiley.
Hoppe, R. (1979). *Z. Kristallogr.* **150**, 23–52.
Hoppe, R., Voigt, S., Glaum, H., Kissel, J., Müller, H. P. & Bernet, K. (1989). *J. Less-Common Met.* **156**, 105–122.

Hugh-Jones, D. A. & Angel, R. J. (1994). *Am. Mineral.* **79**, 405–410.
Ito, J. (1968). *Am. Mineral.* **53**, 1663–1673.
Ito, T. (1935). *Z. Kristallogr.* **90**, 151–162.
Ito, T. (1950). *X-ray Studies on Polymorphism.* Tokyo: Maruzen Co.
Kudoh, Y., Takeda, H. & Ohashi, H. (1989). *Mineral. J.* **14**, 383–387.
Levien, L. & Prewitt, C. T. (1981). *Am. Mineral.* **66**, 315–323.
Makovicky, E. & Balić Žunić, T. (1998). *Acta Cryst.* B**54**, 766–773.
Morimoto, N., Kamajima, Y., Syono, Y., Akimoto, S. & Matui, Y. (1975). *Acta Cryst.* B**31**, 1041–1049.
Ohashi, H. (1988). *J. Jpn. Ass. Min. Petr. Econ. Geol.* **83**, 440–442.
Ohashi, H. (1999*a*). *J. Jpn. Ass. Min. Petr. Econ. Geol.* Submitted.
Ohashi, H. (1999*b*). In preparation.
Ohashi, H., Fujita, T. & Osawa, T. (1982). *J. Jpn. Ass. Min. Petr. Econ. Geol.* **77**, 305–309.
Ohashi, H., Fujita, T. & Osawa, T. (1983). *J. Jpn. Ass. Min. Petr. Econ. Geol.* **78**, 159–163.
Ohashi, H., Osawa, T. & Sato, A. (1990). *Acta Cryst.* B**46**, 742–747.
Ohashi, H., Osawa, T. & Sato, A. (1994*a*). *Acta Cryst.* C**50**, 838–840.
Ohashi, H., Osawa, T. & Sato, A. (1994*b*). *Acta Cryst.* C**50**, 1652–1655.
Ohashi, H., Osawa, T. & Sato, A. (1995). *Acta Cryst.* C**51**, 2476–2477.
Ohashi, H., Osawa, T., Sato, A. & Onoda, Y. (1995). *J. Jpn. Ass. Min. Petr. Econ. Geol.* **90**, 327–332.
Ohashi, H., Osawa, T., Sato, A. & Tsukimura, K. (1996). *J. Jpn. Ass. Min. Petr. Econ. Geol.* **91**, 21–27.
Ohashi, H., Osawa, T. & Tsukimura, K. (1987). *Acta Cryst.* C**51**, 605–607.
Ohashi, Y. (1984). *Phys. Chem. Mineral.* **10**, 217–229.
Ohashi, Y. & Burnham, C. W. (1973). *Am. Mineral.* **58**, 843–849.
Olesch, M., Doroshev, A. M. & Nechaev, P. Ju. (1982). *Neues Jahrb. Miner. Monatsh.* pp. 312–320.
Pauling, L. (1929). *J. Am. Chem. Soc.* **51**, 1010–1026.
Phillips, J. C. (1980). *Phys. Status Solidus B*, **101**, 473–479.
Prewitt, C. T. & Burnham, C. W. (1966) *Am. Mineral.* **51**, 956–975.
Pyatenko, Yu. A. (1973). *Sov. Phys. Crystallogr.* **17**, 677–682.
Robinson, K., Gibbs, G. V. & Ribbe, P. H. (1971). *Science*, **172,** 567–570.
Sasaki, S., Fujino, K., Takéuchi, Y. & Sadanaga, R. (1980). *Acta Cryst.* A**36**, 904–915.
Sasaki, S., Takéuchi, Y., Fujino, K. & Akimoto, S. (1982). *Z. Kristallogr.* **158**, 279–297.
Sato, A., Osawa, T. & Ohashi, H. (1994) *Acta Cryst.* C**50**, 487–488.
Satto, C., Millet, P. & Galy, J. (1997). *Acta Cryst.* C**53**, 1727–1728.
Sedlacek, P., Zedler, A. & Reinecke, K. (1979). *Kristallogr. Technik*, **14**, 1055–1062.
Shannon, R. D. & Prewitt, C. T. (1970) *Acta Cryst.* B**26**, 1046–1048.
Smyth, J. R. (1969). *Mineral. Soc. Am. Spec. Pap.* **2**, 3–29.
Smyth, J. R. (1973). *Am. Mineral.* **58**, 636–648.
Smyth, J. R. (1974). *Am. Mineral.* **59**, 1069–1082.
Sueno, S., Cameron, M. & Prewitt, C. T. (1976). *Am. Mineral.* **61**, 38–53.
Syono, Y., Akimoto, S.-I. & Matsui, Y. (1971). *J. Solid State Chem.* **3**, 369–380.
Takeda, H. (1972). *J. Geophys. Res.* **77**, 5798–5811.
Takeda, H. (1980). *J. Jpn. Ass. Min. Petr. Econ. Geol.* Spec. Issue **2**, 303–317 (in Japanese, with English abstract).
Thorpe, M. F. (1983). *J. Non-Crystal. Solids*, **57**, 355–370.
Tokonami, M., Horiuchi, H., Nakano, A., Akimoto, S.-I. & Morimoto, N. (1979). *Mineral. J.* **9**, 424–426.
Trömel, M. (1983). *Acta Cryst.* B**39**, 664–669.
Trömel, M. (1984). *Acta Cryst.* B**40**, 338–342.
Trömel, M. (1986). *Acta Cryst.* B**42**, 138–141.
Weiss, A., Rieder, M. & Chmielovà, M. (1992). *Eur. J. Mineral.* **4**, 665–682.
Wenger, M. & Armbruster, T. (1991). *Eur. J. Mineral.* **3**, 387–399.
Zhang, L., Ahsbahs, H., Hafner, S. S. & Kutoglu, A. (1997). *Am. Mineral.* **82**, 245–258.
Zhang, L. & Hafner, S. S. (1994). *Am. Mineral.* **79**, 462–473.